04 May 2013, 10:30 am - 11:30 am

Lessons from the Seismic Performance of Pile-Supported Bridges Affected by Liquefaction During the M8.8 2010 Maule Chile Earthquake

Christian Ledezma

Pontificia Universidad Católica de Chile, Chile

Commemorate the Legacy of Ralph B. Peck
April 29 - May 4, 2013 CHICAGO
Seventh International Conference on
Case Histories in Geotechnical Engineering
and Symposium in Honor of Clyde Baker

LESSONS FROM THE SEISMIC PERFORMANCE OF PILE-SUPPORTED BRIDGES AFFECTED BY LIQUEFACTION DURING THE M8.8 2010 MAULE CHILE EARTHQUAKE

Christian Ledezma
Pontificia Universidad Católica de Chile
Vicuña Mackenna 4860, Macul, Santiago, Chile

ABSTRACT

Ground failure case studies have been the source of the most important advances in geotechnical earthquake engineering over the past 50 years. Documented case histories from the 2010 M8.8 Maule Chile earthquake will, if carefully studied, further advance this field. The 2010 M8.8 earthquake in Chile showed that liquefaction-induced soil-foundation-structure interaction problems are still far from being completely understood. The observed damage and partial collapse of pile-supported bridges like Juan Pablo II, Llacolén, Tubul, La Mochita, and Raqui, is most likely due to the effects of liquefaction-induced lateral and vertical ground displacement, which often causes large ground deformations that impose kinematic loads on the pile foundations. In this paper, simplified back-analyses regarding the seismic performance of bridges Mataquito, Juan Pablo II, and Llacolen are presented. The bridges have been selected not only because clear evidence of liquefaction was found at their respective locations, but also because their seismic performance was very different, ranging from little to negligible damage to a larger and more distributed level of damage.

INTRODUCTION

In this paper, three bridge damage cases investigated by the Geotechnical Extreme Events Reconnaissance (GEER) teams during several visits in 2010 are presented. The observations provided herein are based on the GEER report edited by Bray and Frost (2010) and on the paper by Ledezma et al. (2012). The interested reader is referred to those publications for additional details of these and other cases related to the transportation infrastructure.

Two of the three bridges presented in this paper cross the Bío-Bío River, which is the second longest river in Chile. It originates in the Andes and flows 380 km to the Gulf of Arauco on the Pacific Ocean. It is also the widest river in Chile, with an average width of 1 km, and a width of more than 2 km prior to discharging into the ocean. Close to the Pacific Ocean, the river traverses the metropolitan area of Concepción, Chile's second largest metropolitan area; which includes the cities of Talcahuano, San Pedro de la Paz, Lota, and Coronel. Although the Bío-Bío River was once navigable by ship up to the City of Nacimiento, over-logging during the twentieth century led to heavy erosion that has choked the river with silt and rendered it impassable to ship traffic. Near Concepción, the river behaves as a meandering river with fine-grained material deposited on the floodplains. In Concepción, the river is crossed by five bridges: Llacolén Bridge (opened in 2000), Juan Pablo II Bridge (1973), La Mochita Bridge (2005), Puente Viejo Bridge (Old Bío-Bío Bridge, 1942) and Bío-Bío Railroad Bridge (1889). During the 2010 Maule earthquake, all of these bridges experienced different levels of structural damage, compromising normal business activities in the region. The most common geotechnical failure mechanism observed at these bridges was liquefaction-induced lateral spreading that occurred along both shores of the Bío-Bío River. Lateral spreading contributed to approach fill deformations. The most extensive lateral spreading-induced damage occurred on the Concepción end of Llacolén and Juan Pablo II bridges. These two cases, along with the case of Mataquito Bridge, near Iloca (to the north of the epicenter area), are described and analyzed in this paper (Fig. 1).

Liquefaction Susceptibility

Liquefaction susceptibility was evaluated at the three bridge sites using the Standard Penetration Test (SPT) profiles obtained before or after the earthquake, which were provided by the Ministry of Public Works (MOP). The sand liquefaction triggering relationship of Youd et al. (2001) was used to define an approximate normalized SPT threshold value for the occurrence of liquefaction. As recorded peak ground

accelerations in downtown Concepción were about 0.4g (Boroschek et al., 2010), and assuming that these soils may have a fines content on the order of 5% to 15%, an average stress reduction coefficient of about 0.9, a magnitude scaling factor of 0.75, and a total-to-effective vertical stress ratio of about 2, the Youd et al. (2001) procedure estimates that sands with normalized SPT values below approximately 28 blows/foot were likely to liquefy in this event.

Fig. 1. Location and pre-earthquake photos of the three selected bridges.

Liquefaction Effects

Effects of liquefaction-induced lateral spreading were evaluated using the simplified design procedure proposed in the MCEER/ATC-49-1 recommended seismic design document of bridges (ATC/MCEER Joint Venture, 2003). Some of the principal steps involved in this design procedure are:

1. Identify the soil layers that are likely to liquefy.
2. Assign undrained residual strengths (S_{ur}) to the layers that liquefy. Perform pseudo-static seismic stability analysis to calculate the yield coefficient (k_y) for the critical potential sliding mass.
3. Estimate the maximum lateral ground displacement.
4. If the assessment indicates that movement of the foundation is likely to occur in concert with the soil, then the structure should be evaluated for adequacy at the maximum expected displacement. This is the mechanism illustrated in Fig. 2. The structural remediation alternative makes use of the pinning action of the piles.
5. Identify the plastic mechanism that is likely to develop as the ground displaces laterally.
6. From an analysis of the pile response to a liquefaction-induced ground displacement field, the likely shear resistance of the foundation is estimated. This increased resistance is then incorporated into the stability analysis, which increases k_y.
7. Recalculate the overall displacement on the basis of the revised resistance levels, and iterate until the resistance is consistent with the level of displacement estimated. Once a realistic displacement is calculated, the foundation and structural system can be assessed for this level of movement.

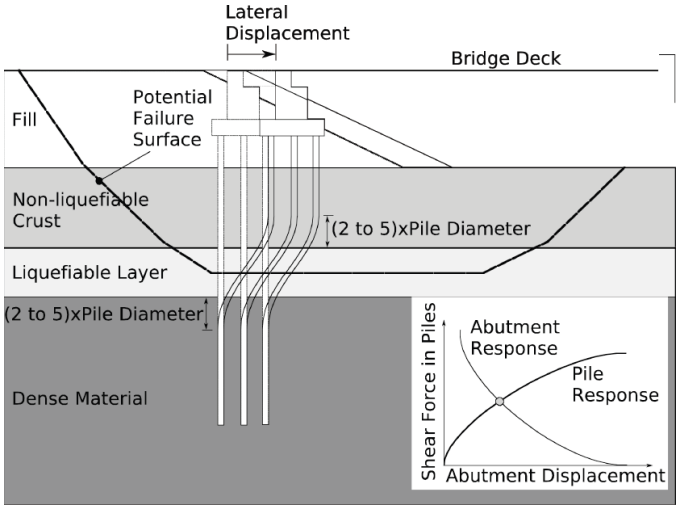

Fig. 2. "Pile-pinning" effect for the case of a pile that is locked into to both the soils above and below the liquefiable soil layer.

In addition to the previous analysis, liquefaction-induced vertical settlements were evaluated at the Juan Pablo II Bridge using the software WSliq (Kramer, 2008). WSliq is a computer program that was developed by a group of researchers at the University of Washington, for the Washington State Department of Transportation, to aid in the evaluation of earthquake-induced soil liquefaction hazards. Using WSliq, the SPT profiles of Juan Pablo II were combined with information about the intensity of the ground motion (PGA=0.4g, Mw=8.8, and R≈100 km) to estimate liquefaction-induced vertical settlements using the models by Tokimatsu and Seed (1987), Ishihara and Yoshimine (1992), Shamoto et al. (1998), and Wu and Seed (2004).

MATAQUITO BRIDGE

The Mataquito Bridge is a 320 m-long, 8-span, reinforced concrete structure that crosses the Mataquito River close to the Pacific Ocean. Each abutment of this bridge was supported by four drilled shafts of circular section (see Fig. 3).

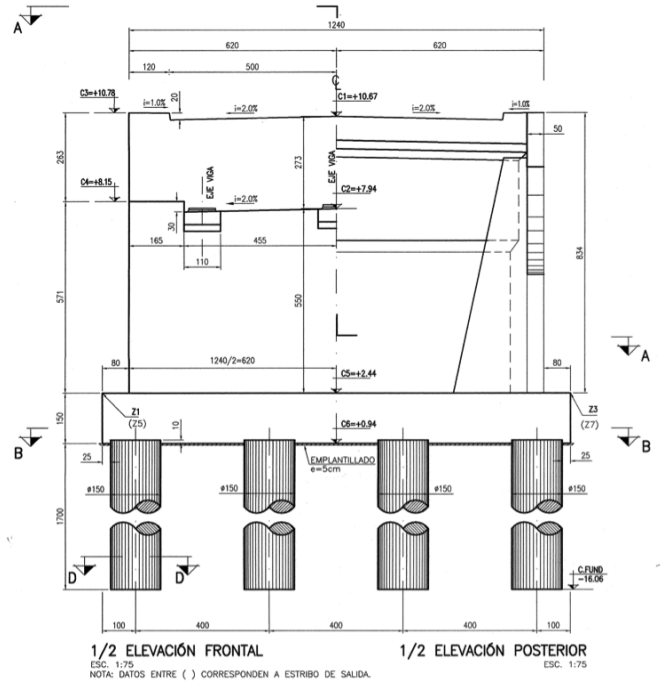

Fig. 3. Elevation view of abutment at Mataquito Bridge (dimensions in cm).

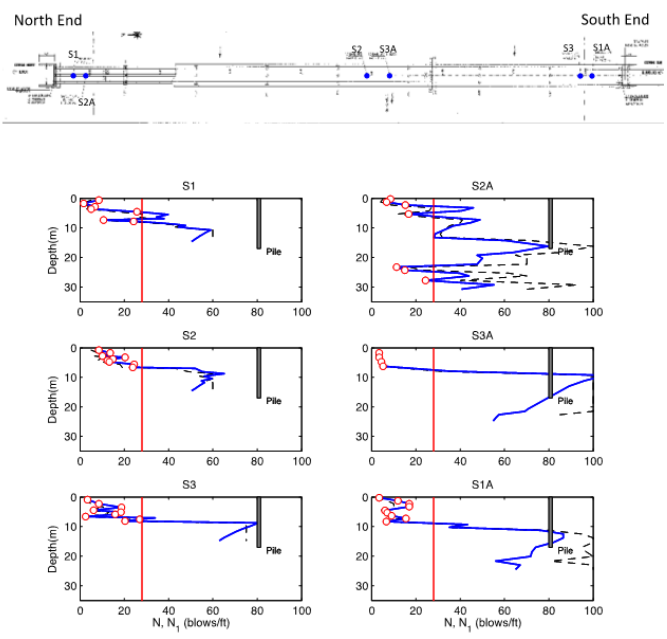

Fig. 4. SPT profiles and liquefiable layers along the Mataquito Bridge. Red circles represent liquefiable layers. The thick blue line is the $N_{1,60}$ profile, while the thin dashed black line represents the $N_{measured}$ profile (assumed = N_{60}).

The north approach was founded on alluvial sediments that liquefied and spread towards the river, causing moderate to significant transverse and longitudinal deformations in the approach fill. In contrast, the south approach was founded on dune sands over possibly shallow bedrock and exhibited negligible deformations. Lateral spreading occurred around both north and south bridge bents but the deformations appear to have been limited by the "pinning" effect from the pile foundations, as the lateral deformation of the ground behind the bridge foundation was essentially zero, while just outside the pile caps these deformations were in the order of 1 to 2 m. Despite evidence of liquefaction at both abutments of this bridge, its structure remained undamaged and functional, and the residual displacements of the bridge foundations were insignificant. As Fig. 4 shows, soil conditions at the north (Iloca) abutment consist of 5 m of liquefiable fine sand with SPT values ranging from 5 to 20 blows/foot, underlain by a layer of fine compact sand 9 m thick, which in turn is underlain by sandy gravel (Boring S1 in Fig. 4). Soil conditions at the south (Quivolgo) abutment consist of 9 m of liquefiable fine sand with SPT values below 10 blows/foot, underlain by a layer of fine compact sand 4 m thick, which in turn is underlain by sandy gravel (Boring S1A in Fig. 4).

Lateral spreading on the south abutment appeared to be more confined, probably due to a combination of the topography of the area and the "pile-pinning" effect. In contrast, on the north side, and due to the large extent of the fields that surround the bridge, moderate to significant lateral spreading was observed extending landward 270 m from the river edge. Lateral spreading from the edge of the abutment wall to the first row of piers was about 54 cm and the total lateral spreading from the edge of the abutment wall to the river's edge was about 180 cm (over a distance of about 65 m). The approach embankment is about 7.6 m high, and settled about 70 cm relative to the bridge deck. The approach embankment experienced a transverse movement of about 60 cm from the centerline as manifested by cracking of the asphalt over a distance of about 200 m. The locally heaved ground observed at the toe of the embankment indicate soil crust compression, likely as a result of liquefaction of the underlying soil. A bridge girder was partially sheared at the first pier on the north side. The bridge remained in use after the earthquake.

If the 28 blows/foot criterion is used in the case of Mataquito Bridge (Fig. 4), it can be observed that the presence of liquefiable material was confined to the upper 10 meters of the soil deposit, and that this material is underlain by rather competent soils. Given that the piles' length was ~17 meters, the resultant embedment probably provided enough vertical and lateral support for the piles to resist the vertical and lateral

loads, despite the occurrence of liquefaction at shallow depths. It is important to note that the piles' length was likely controlled by the large scour anticipated by the hydrological study that was done for this project.

Slope Stability Analysis

Based on the available geotechnical information, a simple slope stability model of the south abutment was created (Fig. 5).

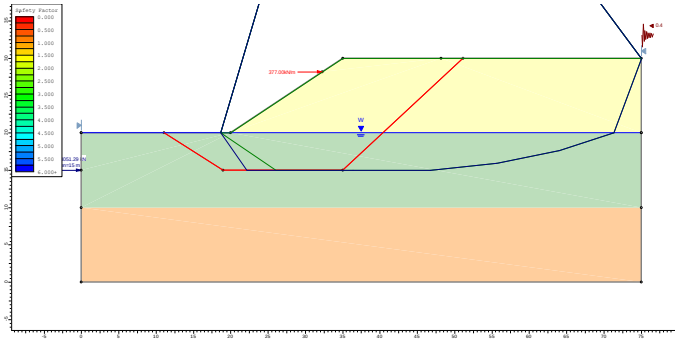

Fig. 5. Post-liquefaction slope stability model for the south abutment of Mataquito Bridge.

In this model, a 10 meters-high earth fill (3H to 2V slope) is underlain by 10 meters of liquefiable material, which in turn is underlain by non-liquefiable material. For the non-liquefiable material properties of γ=22 kN/m3, c'=0 kPa, and ϕ'=40° were considered. For the liquefiable layer, the post-liquefaction undrained shear strength S_{ur} was evaluated using the expression recommended by Ledezma and Bray (2010):

$$\frac{\overline{S_{ur}}}{\sigma_v'} = exp\left(\frac{N_{1,60-cs}}{8} - 3.5\right)\left(1 + \frac{\left(0.3N_{1,60-cs}\right)^2}{128}\right)$$

which is a weighted average of the procedures by Seed and Harder (1990), Olson and Stark (2002), Kramer (2007), and the two correlations of S_{ur} with $N_{1,60\text{-}CS}$, and of S_{ur}/σ_{vc}' with $N_{1,60\text{-}CS}$ proposed by Idriss and Boulanger (2007). Based on the SPT profiles, an average value of $N_{1,60\text{-}CS}$=11 was used to calculate the undrained shear strength profile for the slope stability model.

Additionally, a horizontal force F_{deck}=377 kN/m was included in the analyses to represent the interaction between the abutment wall and the earth fill. This force was located 2H/3 below the earth-fill top, where H is the height of the bridge deck (H=2.73 m). The value of F_{deck} was conservatively calculated using Rankine's model.

The horizontal force P required to reach a factor of safety (FS) of 1.0 was then calculated for horizontal accelerations k_h of 0.05, 0.10, 0.15, 0.20, 0.25, 0.30, and 0.35 (force P was located at the center of the liquefiable layer). Then, the Bray and Travasarou (2007) relationship was used to estimate the lateral displacement associated with each horizontal acceleration, assuming a rigid slope condition (i.e., T_s<0.05s), and considering that M_w=8.8, $S_a(1.5T_s)$=0.4g, and k_y=k_h (since FS=1.0). The result of these analyses is shown in Fig. 6 with colored lines. As Fig. 6 shows, the resulting curve depends on the slope stability procedure that is used. Also, this figure includes the 16% and 84% percentiles from the Bray and Travasarou (2007) relationship.

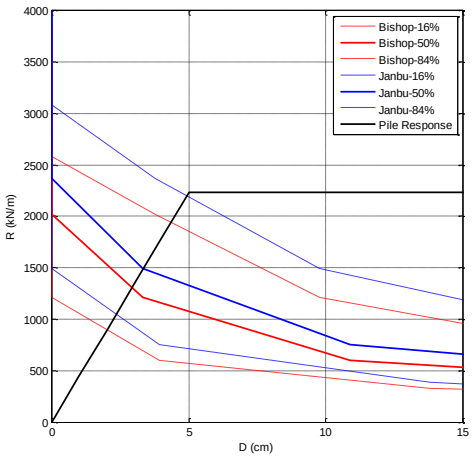

Fig. 6. Expected lateral displacement D for different values of resisting force R in the middle of the liquefiable layer.

Simple, Elastic Pile-Response Analysis

A simple bridge response analysis of Mataquito Bridge's south abutment was performed using an equivalent single-column, with fixities at both ends, to represent the "pile-pinning" effect. An equivalent length equal to the thickness of the liquefiable layer plus two diameters above and below the liquefied soil was used in this analysis. If E is the material's Young modulus, D is the pile's diameter, I is the pile's moment of inertia (i.e., I=$\pi D^4/64$) for a circular pile), and L is the equivalent length of the piles, the shear force and maximum bending moment of the equivalent single-column for a given relative lateral displacement Δ will be

$$V = \frac{12EI}{L^3}\Delta$$

$$M = \frac{6EI}{L^2}\Delta$$

Given that at each abutment there were two rows of piles along the transverse direction of the bridge, and considering a spacing of S (in meters) between piles, the equivalent per-unit-width force R was estimated as R=2V(1/S).

The result of this analysis is shown with a black solid line in Fig. 6. The pile response curve is drawn until the bending moment in the pile section starts to approach the plastic moment. This simplified analysis shows that the expected lateral displacement at this abutment (2 to 5 cm) is relatively consistent with the small to negligible residual lateral displacements observed in the field.

JUAN PABLO II BRIDGE

The Juan Pablo II Bridge is the longest vehicular bridge in Chile, spanning 2,310 m in length. The bridge was opened in 1974. The bridge consists of 70 spans (length = 33 m, width = 21.8 m) each composed of 7 reinforced concrete girders and a concrete deck. Each span sits on reinforced concrete bents with drilled pier supports. Figure 7 shows an elevation view of a pier at Juan Pablo II Bridge.

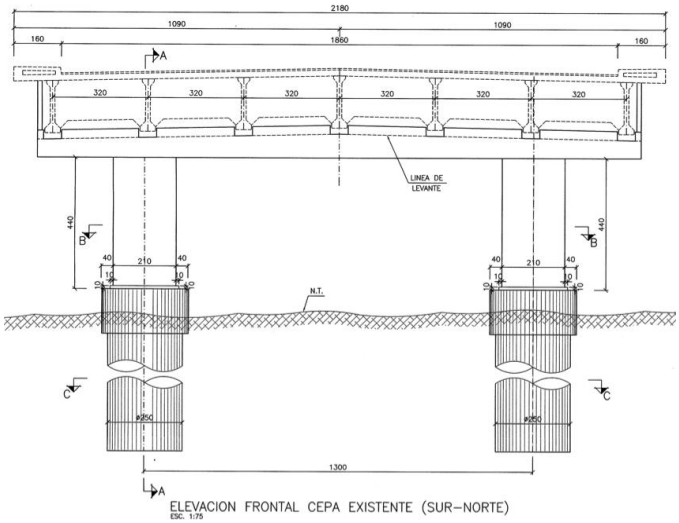

Fig. 7. Elevation view of a pier at Juan Pablo II Bridge (dimensions in cm).

During the earthquake, the bridge suffered severe damage and was closed to the public. Liquefaction and lateral spreading at the northeast approach resulted in significant damage to the bridge superstructure. Most notably, liquefaction caused large settlements at support piers and lateral displacement of the bridge deck (figures 8 and 9). Visual inspection of the surrounding soils indicated the presence of fine loose sands. Several sand boil deposits with diameters in the order of 1 to 10 meters were observed near the structure on both sides of the approach embankment.

Column shear failure, vertical displacements of the bridge deck of up to 1 m, and rotation of the bridge bent of 1° to 3° occurred at the northeast approach (Fig. 9). In contrast with the damage observed at the northeast approach, the southwest approach suffered minor damage. This may be due to a combination of different soils conditions and more gentle slopes observed at the southwest approach.

Fig. 8. Liquefaction-induced vertical settlement along the Juan Pablo II Bridge.

Fig. 9. Failed pier at the north end of the Juan Pablo II Bridge.

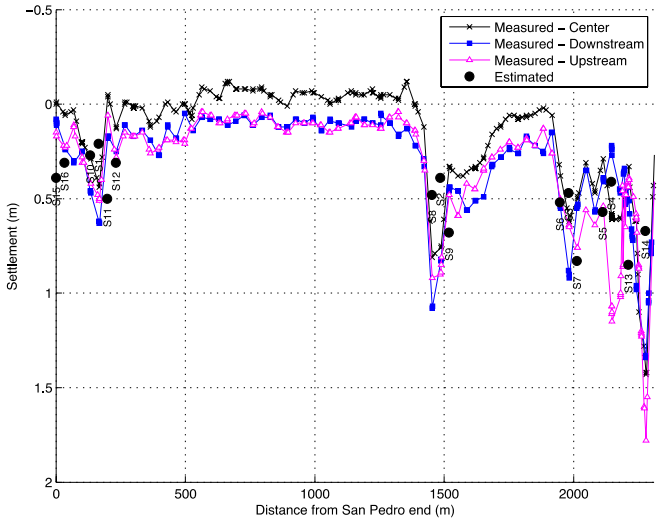

Fig. 10. Measured and estimated settlements along the Juan Pablo II Bridge.

Pier settlements of 0.4 m to 1.5 m were observed at several locations along the bridge (Fig. 10). The bridge deck accommodated these settlements with large vertical deformations, however relatively minor damage of the asphaltic layer was observed. As Fig. 10 shows, settlements of some piers were sometimes larger on the upstream or downstream side, indicating rotation of these bents about the longitudinal axis of the bridge. Soil in the vicinity of the piers showed evidence of ejected water and sand, while soil immediately surrounding the pier was depressed with standing water covering an annular zone around the pier.

The resultant profile of average estimated settlements is also depicted in Figure 10 using black circles. The reasonably good agreement between the estimated and measured deformations suggests that the vertical settlement profile along the Juan Pablo II Bridge can be partially explained by a combination of insufficient end bearing support of the piles and a down-drag effect of the liquefied material that surrounded the piles.

Standard Penetration Test (SPT) profiles obtained after the earthquake close to the north abutment are shown in Fig. 11. Using the 28 blows/foot criterion described in the introduction, distinct layers of liquefiable material (marked with open red circles in Fig. 11) can be observed at the north end of Juan Pablo II Bridge. Note that the soil below the tip of the piles likely liquefied during this event.

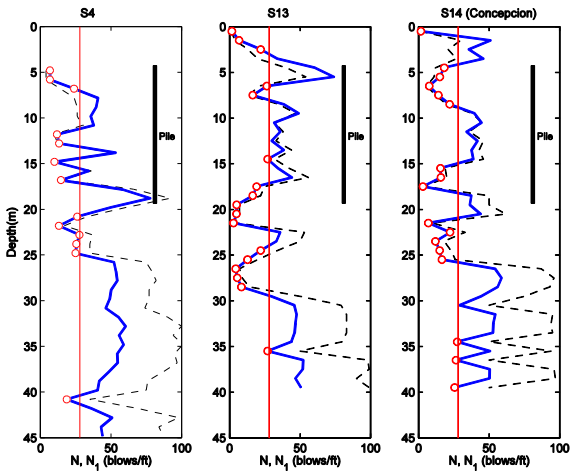

Fig. 11. SPT profiles and liquefiable layers at the north end of the Juan Pablo II Bridge. Red circles represent liquefiable layers. The thick blue line is the $N_{1,60}$ profile, while the thin dashed black line represents the Nmeasured profile (assumed = N_{60}).

Slope Stability Analysis

Based on the available geotechnical information, a simple slope stability model of the north abutment was created (Fig. 12).

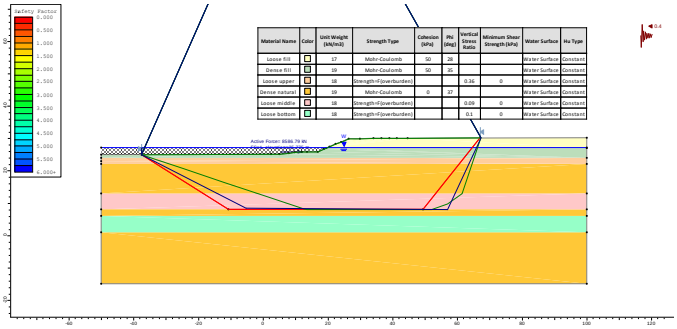

Fig. 12. Post-liquefaction slope stability model for the north abutment of Juan Pablo II Bridge.

In this model a ~6 meters-high non-liquefiable layer is underlain by a sequence of liquefiable (L) and non-liquefiable (NL) layers, approximately: 2 m of L, then 9 m of NL, 5 m of L, 2 m of NL, 5 m of L, and NL material for larger depths. The fill material was modeled using properties γ=17 kN/m3, c'=0 kPa, and ϕ'=28° for the upper part, and γ=19 kN/m3, c'=0 kPa, and ϕ'=35° for the lower one. The parameters used for the dense natural soil were γ=19 kN/m3, c'=0 kPa, and ϕ'=27°. Similar to the case of Mataquito Bridge, the post-liquefaction

undrained shear strength S_{ur} was evaluated using the expression recommended by Ledezma and Bray (2010). Based on the SPT profiles, average values of $N_{1,60\text{-}CS}$=22, 10, and 11 were used to calculate the undrained shear strength for the upper, middle, and bottom liquefiable layers, respectively.

The horizontal force P required to reach a factor of safety (FS) of 1.0 was then calculated for horizontal accelerations k_h of 0.05, 0.10, 0.15, 0.20, 0.25, 0.30, and 0.35 (force P was located at the elevation of the pile cap, see next sub-section). Then, the Bray and Travasarou (2007) relationship was used to estimate the lateral displacement associated with each horizontal acceleration, assuming a rigid slope condition (i.e., T_s<0.05s), and considering that M_w=8.8, $S_a(1.5T_s)$=0.4g, and $k_y=k_h$ (since FS=1.0). The result of these analyses is shown in Fig. 13. This figure shows that, in this case, the resulting curve is relatively insensitive to the slope stability procedure that is used. Also, this figure includes the 16% and 84% percentiles from the Bray and Travasarou (2007) relationship.

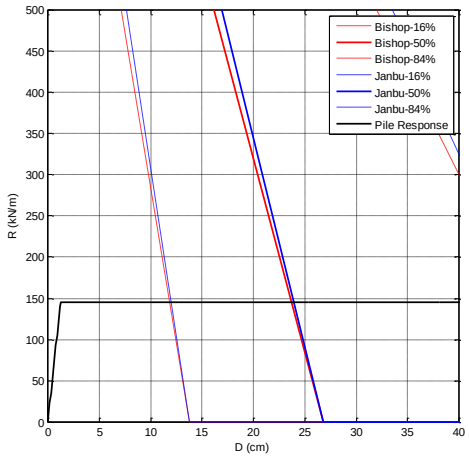

Fig. 13. Expected lateral displacement D for different values of resisting force R acting at the pile cap level.

Simple, Elastic Bridge-Response Analysis

A simple bridge response analysis of Juan Pablo II Bridge's north end was performed using an equivalent single-column. Since the bottom portion of the potential failure surface goes below the tip of the supporting piles (see figures 11 and 12), it seems that the pile-pinning effect could not take place in this case, and that the main structural element supporting the lateral spreading of the non-liquefied soils was the bridge's pier (Fig. 9). This element was modeled as fixed against rotation at the connection with the bridge deck and as free to rotate at the pile cap. Using the same notation as in the case of Mataquito Bridge, the shear force of the equivalent single-column for a given relative lateral displacement Δ will be

$$V = \frac{3EI}{L^3}\Delta$$

Given that there is only one of row of columns at each pier, and considering a spacing of S (in meters) between columns, the equivalent per-unit-width force R was estimated as R=V(1/S).

The result of this analysis is shown with a black line in Fig. 13. This simplified analysis shows that the expected lateral displacement at this abutment (>20 cm) is consistent with the shear failure of the supporting column (Fig. 9).

LLACOLÉN BRIDGE

The Llacolén Bridge in Concepción was constructed in the year 2000 and it spans 2,160 m across the Bío-Bío River, supporting four lanes of vehicular as well as pedestrian access to downtown Concepción. As FHWA (2011) indicates, the bridge is a multispan, simply supported concrete girder bridge. Each span consists of a deck slab and six precast prestressed girders that are supported on two five-column bents with an inverted-T cap beam. Two seismic bars are provided between each pair of adjacent girders. In contrast to the Juan Pablo II Bridge, the average piles' length in the Llacolén Bridge was ~22 m.

During the earthquake, lateral spreading at the northeast approach unseated the bridge deck at its shoreline support, forcing closure of the bridge until a temporary deck could be erected. Ground damage at this approach was observed to extend inland into the southbound traffic lane of Calle Nueva road and continuing hundreds of meters northward and southward along a pedestrian walkway. Calle Nueva parallels the riverbank and runs under the bridge approach. Lateral spreading toward the river caused sufficient displacement to unseat the west and eastbound bridge deck. Closely-spaced (0.1 to 0.2 m on center) flexural cracks on the riverside face of the 1.5 m diameter support columns were observed near the ground surface. The distribution of flexural cracking was more severe for those columns supporting the unseated deck; however, all columns at the north riverbank support experienced flexural cracking at their construction joint (between 2-2.5 m above ground surface). Ground settlement of 0.25-0.30 m also occurred at each of the exit ramp bents. According to FHWA (2011), the nearby ground settled up to 0.4 m and experienced significant shaking, resulting in a 0.25-m separation between the columns and the surrounding ground. Terrestrial LIDAR measurements performed after the earthquake (Kayen, 2012) show that the relative horizontal

displacement of the columns with respect to their bases varied from 0 and 12 cm away from the river at the columns in the shoreline support, while the second and third rows of columns experienced, a rather uniform displacement of their upper ends of 11 cm and 16 cm respectively, towards the river.

If the 28 blows/foot criterion is used in the case of Llacolén Bridge (Figure 14), two main observations can be made. First, with the clear exception of boring S6, the presence of liquefiable material was rather limited when compared to the case of the Juan Pablo II Bridge. And second, the piles' length was enough to provide good end bearing support for most of the piles, despite the occurrence of liquefaction at some depths along the piles. At the north approach, where earthquake-induced damage was concentrated, Boring S-6 indicates that liquefiable soils were present at different depths in the first 20 meters of soil deposit, with the exception of the 9 to 12 m deep zone, were a layer of non-liquefiable material was present.

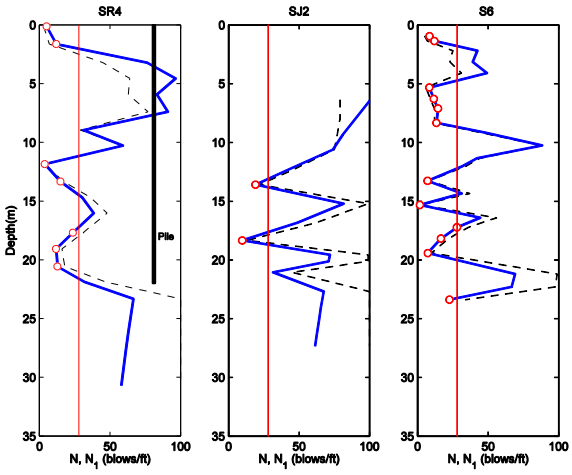

Fig. 14. SPT profiles and liquefiable layers close to the north end of the Llacolén Bridge. Red circles represent liquefiable layers. The thick blue line is the $N_{1,60}$ profile, while the thin dashed black line represents the $N_{measured}$ profile (assumed = N_{60}).

Slope Stability Analysis

Similar to the previous cases, a simple slope stability model of the north abutment was created (Fig. 15).

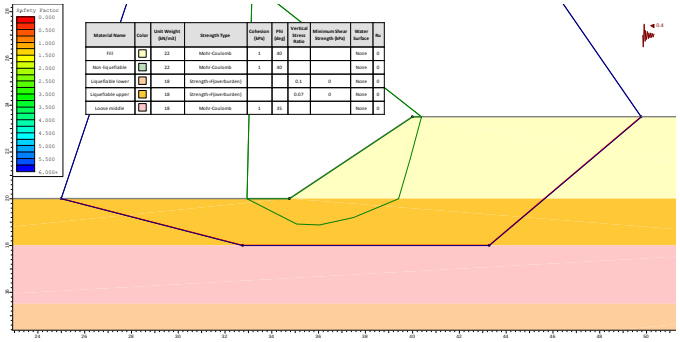

Fig. 15. Post-liquefaction slope stability model for the north abutment of Llacolen Bridge.

In this model, a 3.5 meters-high (note: estimated height) of non-liquefiable fill is underlain by a sequence of liquefiable (L) and non-liquefiable (NL) layers, approximately: 2 m of L, then 2.5 m of loose NL, 4.5 m of L, and loose to NL material for larger depths. The fill material was modeled using properties γ=22 kN/m3, c'=0 kPa, and ϕ'=40°. The parameters used for the loose non-liquefiable natural soil were γ=18 kN/m3, c'=0 kPa, and ϕ'=35°. Similar to the case of Mataquito Bridge, the post-liquefaction undrained shear strength S_{ur} was evaluated using the expression recommended by Ledezma and Bray (2010). Based on the SPT profiles, average values of $N_{1,60\text{-}CS}$=6 and 11 were used, respectively, to calculate the residual undrained shear strength for the liquefiable layers above and below the upper loose non-liquefiable layer.

The horizontal force P required to reach a factor of safety (FS) of 1.0 was then calculated for horizontal accelerations k_h of 0.05, 0.10, 0.15, 0.20, 0.25, 0.30, and 0.35 (force P was at the center of the top liquefiable layer). Then, the Bray and Travasarou (2007) relationship was used to estimate the lateral displacement associated with each horizontal acceleration, assuming a rigid slope condition (i.e., T_s<0.05s), and considering that M_w=8.8, $S_a(1.5T_s)$=0.4g, and $k_y=k_h$ (since FS=1.0). The result of these analyses is shown in Fig. 16. This figure shows that, in this case, the resulting curve is relatively insensitive to the slope stability procedure that is used. Also, this figure includes the 16% and 84% percentiles from the Bray and Travasarou (2007) relationship.

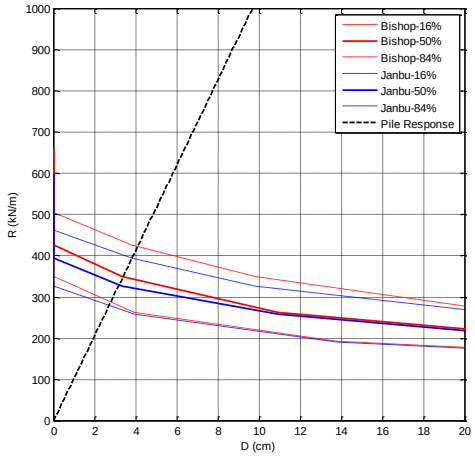

Fig. 16. Expected lateral displacement D for different values of resisting force R acting at the pile cap level.

Simple, Elastic Bridge-Response Analysis

A simple bridge response analysis of Llacolen Bridge's north end was performed using an equivalent single-column, with fixities at both ends, to represent the "pile-pinning" effect. An equivalent length equal to the total thickness of the top liquefiable layers (~9 m) plus two pile diameters was used in this analysis. Using the same notation as in the case of Mataquito Bridge, the shear force of the equivalent single-column for a given relative lateral displacement Δ will be

$$V = \frac{12EI}{L^3}\Delta$$

Given that there is only one of row of piles at each pier, and considering a spacing of S (in meters) between columns, the equivalent per-unit-width force R was estimated as R=V(1/S).

The result of this analysis is shown with a black line in Fig. 16. This simplified analysis shows that the expected lateral displacement at this abutment (2 to 4 cm) is relatively consistent with the small to moderate residual lateral displacements observed in the field.

CONCLUSIONS

Key observations regarding the seismic performance of three bridges affected by the M8.8 2010 Maule Chile Earthquake were presented, namely: Mataquito Bridge, Juan Pablo II, and Llacolén Bridge. These three bridges have been selected not only because clear evidence of liquefaction was found at their respective locations, but also because their seismic performance was very different, ranging from little to none damage, like in the case of Mataquito Bridge, to a larger and more distributed level of damage like in the case of Juan Pablo II Bridge. Liquefaction susceptibility and liquefaction effects, in terms of vertical settlements and lateral spreading, were evaluated for each SPT-profile at the bridge sites. The results of the analyzes show that the Youd et al. (2001) liquefaction assessment correlates reasonably well with the observed occurrence of liquefaction at these sites, and that the current expressions used to calculate liquefaction-induced vertical settlements and lateral spreading provide simple yet realistic estimates.

ACKNOWLEDGEMENTS

This research was made possible by grants from (i) the Chilean National Commission for Scientific and Technological Research under Fondecyt de Iniciación Award Number 11110125, (ii) the United States Department of State's Bureau of Educational and Cultural Affairs (ECA) through the Fulbright Program awarded to the author (NEXUS Program), and (iii) the University of Washington's Visiting Scholarship awarded to the author. Any opinions expressed in this material are those of the author. Discussions with Prof. Pedro Arduino from the University of Washington, Seattle, were very useful. The author would also like to thank Carla Serrano, MS student at the Pontificia Universidad Católica de Chile, for compiling the SPT data that was used for this study, and also to the Ministry of Public Works (MOP, Chile) for providing the required data to perform the analyses.

REFERENCES

ATC/MCEER Joint Venture. (2003). "Recommended LRFD guidelines for the seismic design of highway bridges." Liquefaction Study Report No. MCEER/ATC-49-1 Prepared under NCHRP Project 12-49, Applied Technology Council, Multidisciplinary Center for Earthquake Engineering Research, Buffalo, N.Y.

Boroschek, R., Soto, P., and León, R., 2010. Registros del Terremoto del Maule, Mw=8.8, 27 de Febrero de 2010, RENADIC Report 10/05, August 2010.

Bray, J. D. , and Travasarou, T. (2007). "Simplified procedure for estimating earthquake-induced deviatoric slope displacements." J. Geotech. Geoenviron. Eng. , 133 (4), 381–392.

Bray, J.D. and Frost, J.D., Eds., 2010. Geo-engineering Reconnaissance of the 2010 Maule, Chile Earthquake, a report

of the NSF- Sponsored GEER Association Team, primary authors: Arduino et al., http://www.geerassociation.org/.

Federal Highway Administration (FHWA), 2011. Post-Earthquake Reconnaissance Report on Transportation Infrastructure: Impact of the February 27, 2010, Offshore Maule Earthquake in Chile. Authors: Wen-Huei Phillip Yen, Genda Chen, Ian Buckle, Tony Allen, Daniel Alzamora, Jeffrey Ger, and Juan G. Arias. Report No. FHWA-HRT-11-030, March 2011.

Idriss, I.M. and Boulanger, R.W. (2008). Soil liquefaction during earthquakes, EERI Monograph 12, Earthquake Engineering Research Institute, Oakland, California, 262 pp.

Ishihara, K. and Yoshimine, M. (1992). "Evaluation of settlements in sand deposits following liquefaction during earthquakes," Soils and Foundations, Vol. 32, No. 1, pp. 173-188.

Kayen, R., 2012. Personal communication. January, 2012.

Kramer, S.L. (2008). "Evaluation of Liquefaction Hazards in Washington State". Washington State Transportation Center (TRAC) Report. December, 2008.

Kramer, S.L. and Baska, D.A. (2009). "Estimation of permanent displacement due to lateral spreading," Journal of Geotechnical and Geoenvironmental Engineering, ASCE, accepted pending revisions.

Kramer, S.L., 20007. Personal communication.

Ledezma, C. and Bray, J. (2010). "Probabilistic Performance-Based Procedure to Evaluate Pile Foundations at Sites with Liquefaction-Induced Lateral Displacement." J. Geotech. Geoenviron. Eng., 136(3), 464–476.

Ledezma, C., Hutchinson, T., Ashford, S., Moss, R.E.S., Arduino, P., Bray, J.D., Olson, S.M., Hashash, Y., Verdugo, R., Frost, D., Kayen, R., and Rollins, L (2012). "Effects of Ground Failure on Bridges, Roads, and Railroads". Earthquake Spectra: June 2012, Vol. 28, No. S1, pp. S119-S143.

Olson, S. M., and Stark, T. D. (2002). "Liquefied strength ratio from liquefaction flow failure case histories." Can. Geotech. J. , 39 , 629–647.

Seed, R. B. , and Harder, L. F. (1990). "SPT-based analysis of cyclic pore pressure generation and undrained residual strength." Proceedings of H. Bolton Seed Memorial Symposium , Vol. 2 , BiTech Pub, Ltd., Vancouver, BC, Canada, 351–376.

Shamoto, Y., Zhang, J.-M., and Tokimatsu, K. (1998). "Methods for evaluating residual post-liquefaction ground settlement and horizontal displacement," Soils and Foundations, Special Issue No. 2, 69-83.

Tokimatsu, K. and Seed, H.B. (1987). "Evaluation of settlements in sand due to earthquake shaking," Journal of Geotechnical Engineering, ASCE, Vol. 113, No. 8, pp. 861-878.

Wu, J. and Seed, R.B. (2004). "Estimation of liquefaction-induced ground settlement (case studies)," Proceedings, Fifth International Conference on Case Histories in Geotechnical Engineering, New York, pp. 1-8.

Youd, T.L., Hansen, C.M., and Bartlett, S.F. (2002). "Revised multilinear regression equations for prediction of lateral spread displacement", J. Geotech. Geoenviron. Eng., ASCE, 128(12), 1007-1017.

Youd, T.L., I. M. Idriss, Ronald D. Andrus, Ignacio Arango, Gonzalo Castro, John T. Christian, Richardo Dobry, W. D. Liam Finn, Leslie F. Harder Jr., Mary Ellen Hynes, Kenji Ishihara, Joseph P. Koester, Sam S. C. Liao, William F. Marcuson III, Geoffrey R. Martin, James K. Mitchell, Yoshiharu Moriwaki, Maurice S. Power, Peter K. Robertson, Raymond B. Seed, and Kenneth H. Stokoe II, 2001. Liquefaction Resistance of Soils: Summary Report from the 1996 NCEER and 1998 NCEER/NSF Workshops on Evaluation of Liquefaction Resistance of Soils. Journal of Geotechnical and Geoenvironmental Engineering, 124(10).